A Transient Microsphere Model for Nonlinear Viscoelasticity in Dynamic Polymer Networks

Samuel Lamont
Department of Mechanical Engineering,
University of Colorado, Boulder,
Boulder, CO 80309
e-mail: samuel.lamont@colorado.edu

Franck J. Vernerey[1]
Department of Mechanical Engineering,
Program of Materials Science and Engineering,
University of Colorado, Boulder,
Boulder, CO 80309
e-mail: franck.vernerey@colorado.edu

Viscoelastic material behavior in polymer systems largely arises from dynamic topological rearrangement at the network level. In this paper, we present a physically motivated microsphere formulation for modeling the mechanics of transient polymer networks. By following the directional statistics of chain alignment and local chain stretch, the transient microsphere model (TMM) is fully anisotropic and micro-mechanically based. Network evolution is tracked throughout deformation using a Fokker–Planck equation that incorporates the effects of bond creation and deletion at rates that are sensitive to the chain-level environment. Using published data, we demonstrate the model to capture various material responses observed in physical polymers. [DOI: 10.1115/1.4052375]

Keywords: constitutive modeling of materials, elasticity, failure criteria, mechanical properties of materials, micromechanics

1 Introduction

The mechanical properties of soft polymeric materials feature an enormous range of both fluid-like and solid-like behaviors that are ultimately governed by interactions at the chain and network levels. Materials with supramolecular architecture such as physically bonded polymers are particularly diverse in their properties, despite similarities in the underlying structure. For instance, physical gels have been reported with different levels of viscoelasticity [1–3], self-healing [4,5], and hyperextensibility [6]. These properties can be attributed to the reversibility of physical bonds, which has also been shown to provide sacrificial energy dissipation and increase the toughness of hybrid (covalent and physical) materials [7]. This makes them desirable for a variety of applications, but there remains a large gap in our knowledge of the connection between chemical design and emergent properties. We thus need to gain a deeper understanding of the mechanisms that govern chain kinetics and, perhaps more importantly, how this drives the emergent network response.

While the chemical makeup of many physically bonded networks may be different, the physics that governs their behavior is fundamentally the same. Physical bonds have an activation energy close in magnitude to the thermal background, causing them to break and reform at relatively high rates. This type of reaction is well-described by kinetic theories such as those proposed by Eyring [8] and Kramers [9]. For instance, the rheological properties of some associating polymer solutions were well-described by relating the relaxation timescale of the material to the average lifetime of a bond [10,11]. This material template has remained common for studying the viscoelastic properties of physical networks, but discrepancies in the response are observed even for networks with similar architecture (see works by Erk et al. [12,13], Berret and Séréro [1,14], and Skrzeszewka et al. [3,15]). Further, while much effort has gone into studying the topology of these networks [16,17], there has been little work dedicated to directly characterizing the role of physical bonds. Indeed, a large variety of unique network architectures have been created [18], but their diversity hinders our ability to finely tune the desired mechanical properties. A primary goal of this study is thus to relate the governing physics of different networks to their resultant material behaviors.

Statistical approaches such as the transient network theory (TNT) [19,20] offer a promising template for bridging the connection between chain-level physics and material properties. The TNT is based on tracking the configuration of polymer chains within a network during deformation. With this approach, the behavior of a material can be fully described by knowing the distribution function $\varphi(\mathbf{r})$ of end-to-end vectors $\mathbf{r}$ of polymer chains in the network. While this description was capable of describing the complex mechanics of elastic damage [21] and the rheology of fire ant aggregates [22], it is computationally expensive to track the full distribution $\varphi(\mathbf{r})$ throughout deformation. To combat this, a reduced, tensorial form of the TNT was developed, which instead tracked the covariance $\boldsymbol{\mu}$ of the distribution [20,23]. This has been applied to study a variety of transient behaviors such as biological growth [24], fracture [25], and the mechanics of topological materials [26], but the gain in numerical convenience comes at a loss of directional information. These reduced forms are thus insufficient for properly capturing complex chain-level interactions.

The difficulty in adding complexity to chain-level physics lies in the homogenization method used to bridge chain and network length scales. Many physically based formulations, such as Treloar's three-chains model [27] and the Arruda–Boyce eight-chains model [28], make significant simplifications to the environment felt by a single chain to facilitate convenient constitutive laws. This comes at the cost of a loss in the directional properties of the network, however, which motivated the development of microsphere models that maintain a fully anisotropic description of the network [29–31]. This approach has been used to explore the effects of non-affine deformations [30,32] and provide physical interpretation to the Mullins effect in rubber [31,33]. Current viscoelastic microsphere models are restricted to rubber-like materials such as elastomers [34,35]. These models have done well to capture the time-dependency of topological effects originating from reptation and the release of chain restrictions (entanglements), but the dissipative mechanisms in dynamic polymer systems are quite different [20]. As such, behaviors unique to these materials such as stress overshoot [2,36], self-healing [4,5], and creep [10,14] cannot be described by rubber-like viscoelasticity. Development in this area could thus provide a vital connection between bond characterization and viscoelastic behavior in physically bonded networks.

[1]Corresponding author.

Contributed by the Applied Mechanics Division of ASME for publication in the Journal of Applied Mechanics. Manuscript received June 16, 2021; final manuscript received September 3, 2021; published online October 11, 2021. Assoc. Editor: Sinan Keten.

The goal of this study is to unify experiments and theory in the context of dynamic polymer networks. We propose here a microsphere formulation of the TNT, also known as the transient microsphere model (TMM), which accounts for variable detachment rates. Our contributions are thus two-fold: (i) generalizing the microsphere approach to transient networks and (ii) further supplementing previous works on transient networks by exploring force-dependent bond kinetics. We demonstrate that this formulation is versatile and predicts a large variety of material responses using a minimal parametric space. In Sec. 2, we present the theoretical framework of the model and derive thermodynamically consistent constitutive laws. Section 3 then outlines our solution procedure and is dedicated to exploring the predictions of our model, which begins with defining its limiting cases, and is followed by direct comparisons to published experiments. We finish the paper with concluding remarks and an overview of the limitations and key findings of the model.

2 Theoretical Framework

This section presents a theoretical basis for the TMM. We begin the detailed analysis of our system by considering flexible polymer chains that detach from the network and reattach at given rates. Expanding on our previous works, which have assumed constant rates of attachment and detachment [25,37], we derive a microsphere theory for dynamic networks which incorporates a force-dependent kinetic rate of detachment.

2.1 Nonlinear Chain Statistics.

Let us start by defining the behavior of a single flexible chain. Once attached to the network, a chain of length Nb stores energy according to the stretch of its end-to-end vector $\lambda = r/\sqrt{N}b$. While Gaussian statistics are commonly used for small chain stretches, this is known to be inadequate as a chain is stretched to its contour length. To this end, Kuhn and Grun [38] and James and Guth [39] proposed an energy functional, ψ, based on the inverse Langevin function,

$$\psi = k_b T \sqrt{N}\left(\lambda\beta + \frac{\beta}{\sinh\beta}\right) \tag{1}$$

where $\beta = \mathcal{L}^{-1}(\lambda/\sqrt{N})$ and $\mathcal{L}^{-1}$ is the inverse Langevin function. The energetic penalty of pulling a chain necessitates a restoring force f that seeks to bring the two ends of the chain back to their resting state, $f = \partial\psi/\partial r$. As the inverse Langevin function is highly nonlinear, many ways of approximating the form of these equations have been proposed. One method which has been shown to replicate the function exceptionally well up to its asymptotic limit at $\lambda = \sqrt{N}$ is the Padé approximation presented in Cohen [40],

$$f(\lambda) = \frac{k_b T}{b}\mathcal{L}^{-1}\left(\frac{\lambda}{\sqrt{N}}\right) \quad \text{where } \mathcal{L}^{-1}(x) \approx \frac{x(3 - x^2)}{1 - x^2} \tag{2}$$

Equation (2) predicts that the stiffness of a chain increases nonlinearly as the chain is stretched to its contour length, at which point it diverges to infinity. The force in a chain cannot, of course, be considered infinite, and we would expect the chain to detach from the network before it reaches this limit. In fact, the relatively weak strength of physical bonds causes them to regularly detach from the network and reattach even when no force is being placed on them at all. This sources from a low activation energy ΔE between the attached and detached states of the chain. Clearly, the kinetic rate of detachment k_d and the kinetic rate of attachment k_a must be comparable in size, or a percolated network would not form. On the other hand, these rates must be sensitive to external perturbations for it to be possible to separate the network. This problem was classically studied by Bell [41], who proposed a kinetic rate in the form

$$k_d = \omega_0 \exp\frac{-(\Delta E - f\delta)}{k_b T} \tag{3}$$

where ω_0 is the natural frequency of oscillations in the atoms ($\approx 10^{-13}$ s), f is the external force placed on the bond, and δ is a characteristic length scale of the bonding interaction. The average resting length $\sqrt{N}b$ of a chain in a percolated network produces a finite force even when the material is stress-free; this is attributed to volume-exclusion and incompressibility conditions. Equation (3) thus presents an interesting observation in the context of a chain's resting kinetics, which will certainly be larger for networks of chains than isolated chains. To simplify the parameters of the TMM, we take a similar approach as Tanaka and Edwards [11] and describe k_d in terms of its resting value $k_{d,0}$,

$$k_d = k_{d,0}\exp\frac{f - f_{eq}}{f}, \quad \text{where } k_{d,0} = \omega_0 \exp\frac{f_{eq}\delta - \Delta E}{k_b T} \tag{4}$$

and $f_{eq} = f(1/\sqrt{N})$ is the force in a chain of length $\sqrt{N}b$. The chosen form of k_d therefore enforces the average lifetime of a bond in a stress-free network to be $1/k_{d,0}$. The force sensitivity $f_0 = k_b T/\delta$ is preferred in the exponential term to further simplify notation. Its physical meaning can be interpreted as the relative force-scale on which the respective physical bonding exits. For large values of f_0, the tension in the chain is negligible and the detachment rate remains approximately constant, while smaller values facilitate rapidly increasing chain kinetics. In this work, we normalize f_0 by $b/k_b T$ to enforce a nondimensional scale—unless stated otherwise, the unit for f is $k_b T/b$. Thus, Fig. 1(b) illustrates the exponential curves for $f_0 = 2\ k_b T/b$, $f_0 = 5\ k_b T/b$, and $f_0 = 10\ k_b T/b$.

2.2 The Transient Microsphere Model.

The full transient network theory approach describes the kinematics of a polymer chain by following the distribution P(r) of its end-to-end vector r under external loading. While this provides a wealth of information regarding the chain-level statistics, it can become computationally expensive for the study of macroscopic problems. Conversely, the fully reduced TNT proposed in Refs. [20,37] track only the statistical moments of the distribution and can be solved at the continuum level. They can thus be incorporated into larger-scale simulations using the finite element method [25,42], but the resulting model is fully isotropic. We therefore propose a semi-reduced model in the context of the microsphere formulations originally introduced by Treloar [43] and formalized by Wu and Van der Geissen [29,44]. In this approach, physical quantities of the network are replaced by a single representative chain in each direction, parameterized by their polar and azimuthal angles, φ and θ, respectively. To fully characterize the distribution, we require knowledge of two physical states of the network: the directional chain density $\rho(\theta, \varphi)$ and the directional chain stretch $\lambda(\theta, \varphi)$.

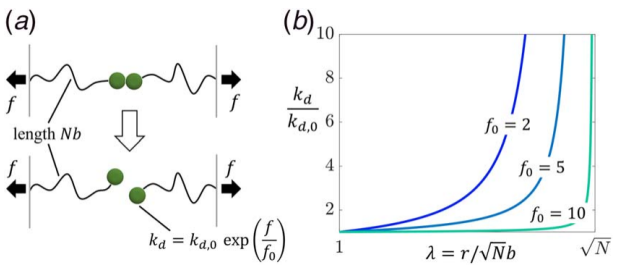

Fig. 1 (a) Two polymer chains with resting length $\sqrt{N}b$ which detach at a rate k_d and (b) exponential change in detachment rate as a function of chain length r. f_0 is given in units of $k_b T/b$.

We begin by defining the physical quantities $\rho(\theta, \varphi)$ and $\lambda(\theta, \varphi)$ for a network of flexible chains. Due to chain kinetics, a network with c_t total chains per unit volume has $c \le c_t$ chains connected to the network at any one time. We refer to these chains as "effective" as they store elastic energy, while the corresponding $(c_t - c)$ chains are considered to be dangling chains. As the network deforms, a higher density of chains begins to align in the principal directions of deformation, which corresponds to a higher probability of finding a chain aligned in this direction. The directional density $\rho(\theta, \varphi)$ quantifies this alignment and is found by taking the average number of chains aligned in a given direction,

$$\rho(\theta, \varphi) = \int_0^\infty cP(r, \theta, \varphi) r^2 dr \tag{5}$$

The covalent networks considered by Wu and Van der Giessen were assumed to maintain a constant number of attached chains, and we note here that the chain orientation distribution function (CODF) in Ref. [44] is exactly $\rho(\theta, \varphi)/c$. Thus, $\rho(\theta, \varphi)$ represents the number density of chains per unit volume in the solid angle traced out by θ and φ (Fig. 2(c)). To determine the average stretch in a given direction, we first note that we should only consider the stretch of chains currently attached to the network. The directional stretch $\lambda(\theta, \varphi)$ should therefore be normalized by the density of chains currently aligned in a given direction. From this, the directional stretch should be given by

$$\lambda(\theta, \varphi) = \sqrt{\frac{1}{Nb} \frac{\mu(\theta, \varphi)}{\rho(\theta, \varphi)}} \tag{6}$$

where

$$\mu(\theta, \varphi) = \int_0^\infty cP(r, \theta, \varphi) r^4 dr \tag{7}$$

is the directional second moment of the distribution. The directional stretch reflects the average stretch felt by a chain aligned in a given direction. Both quantities $\rho(\theta, \varphi)$ and $\lambda(\theta, \varphi)$ are discretized on the unit sphere S, so that macroscopic quantities can be recovered by integrating over the domain of S. One important quantity that results from our definition of $\rho(\theta, \varphi)$ is the current chain density,

$$c = \int_S \rho(\theta, \varphi) dS, \quad \text{where} \quad \int_S dS = \int_0^{2\pi} \int_0^{\pi} \sin\varphi \, d\varphi \, d\theta \tag{8}$$

For elastic networks, assuming that no chains have ruptured, the density of attached chains is constant, and this integral will always equal c_t, the total chain concentration. We show in Sec. 3.2 that force-accelerated bond kinetics can temporarily decrease the current density of attached chains, causing network softening and energy dissipation.

2.3 Kinematics. Let us now assess the evolution of the quantities $\rho(\theta, \varphi)$ and $\lambda(\theta, \varphi)$ as the network is exposed to a macroscopic deformation. For this, we continue our description of chains in a spherical coordinate system with basis vectors e_r, e_θ, and e_φ. Assuming an instantaneously affine deformation [45], a chain with end-to-end vector $r(r, \theta, \varphi)$ is transformed according to, $\dot{r} = Lr$, where L is the macroscopic velocity gradient. In previous works, we have used a Fokker–Planck equation to track the evolution of $P(r)$ subject to an external velocity gradient [20,37]. Leaving the details for Appendix A, we integrate the Fokker–Planck equation over the radial direction as in Eqs. (5) and (7) and derive the following evolution laws:

$$\frac{\partial \rho}{\partial t} = L : 3\rho(e_r \otimes e_r) - \frac{1}{\sin\varphi} \frac{\partial \rho}{\partial \theta}(e_\theta \otimes e_r) - \frac{\partial \rho}{\partial \varphi}(e_\varphi \otimes e_r) + k_a \rho_0 \frac{c_t}{c} - k_d(\theta, \varphi)\rho \tag{9}$$

$$\frac{\partial \mu}{\partial t} = L : 5\mu(e_r \otimes e_r) - \frac{1}{\sin\varphi} \frac{\partial \mu}{\partial \theta}(e_\theta \otimes e_r) - \frac{\partial \mu}{\partial \varphi}(e_\varphi \otimes e_r) + k_a \mu_0 \frac{c_t}{c} - k_d(\theta, \varphi)\mu \tag{10}$$

where $\otimes$ denotes the dyadic product and ρ_0 and μ_0 are the values of ρ and μ at which chains reattach, respectively. We note here that the bracketed term results from a coordinate transformation between the cartesian velocity gradient L and the spherical basis description of a chain. These equations were also derived with a globally incompressible assumption (with the condition $\mathrm{Tr}\, L = 0$). There are two major contributions to these equations: (i) the distortion of the network by the velocity gradient L and (ii) the difference of chains detaching in their current state to those attaching back in their reference configuration. While the equations are given in rate-form, the chain conformation (represented by ρ and μ) is obtained by integrating them over time. Thus, the history-dependence of the material is dependent on the rate of loading; the competition between the deformation rate and bond dynamics determines whether the network behaves as an elastic solid, viscous fluid, or lies between. In the case of permanent bonds ($k_a = k_d = 0$), these evolution laws describe the directional changes in the distribution of a covalently bonded network. In this scenario, we can show that the TMM converges back to the kinematics of an affine elastic network [20]. The force-sensitive bond kinetics in physical networks creates nonlinear viscoelastic behavior as described by Eq. (4). To capture this, we propose a mean-field approximation by defining the average directional kinetic rate

$$k_d(\theta, \varphi) = k_{d,0} \exp\frac{f(\lambda(\theta, \varphi)) - f_{eq}}{f_0} \tag{11}$$

where the functional form of f is given by the Padé approximation (Eq. (2)). We recognize in Eq. (9), the bond detachment rate, $\xi_d = k_d \rho$, representing the directional density of chains detaching from the network. Its corresponding attachment rate, $\xi_a = k_a(c_t/c - 1)\rho_0$, enforces a global differential equation for the

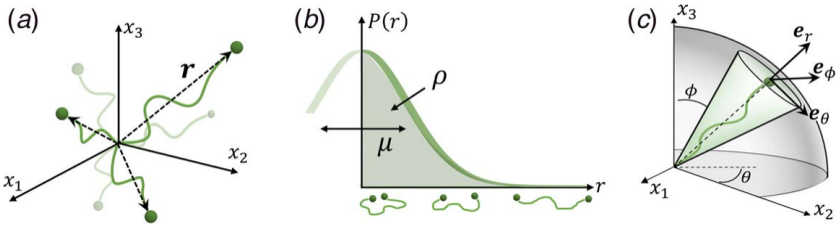

Fig. 2 (a) The full configuration space of a polymer chain of length Nb. (b) The probability distribution P of end-to-end distance r. The directional density ρ is the zeroth moment of the distribution in a given direction, while μ is the second moment. (c) Microsphere discretization of a polymer network. Each direction described by angles θ and φ is represented by an averaged quantity.

density of attached chains in the network. Integrating Eq. (9) over the microsphere, we obtain

$$\dot{c} = \int_S \xi_a - \xi_d(\theta, \varphi) dS \tag{12}$$

In the absence of deformation, the resting kinetics of the network enforce an equilibrium chain concentration c_0, which represents a state of thermodynamic equilibrium between attachment and detachment events. From Eq. (8), it is defined as

$$c_0 = c_t \frac{k_a}{k_{d,0} + k_a} \tag{13}$$

By integrating Eqs. (9) and (10), we can also analytically define the stress-free values of ρ and μ in terms of the initial concentration as

$$\rho_0 = \frac{c_0}{4\pi}, \quad \mu_0 = \frac{c_0 N b^2}{4\pi} \tag{14}$$

From here, the typical resting length of a Gaussian chain is recovered with Eq. (6), yielding $\lambda_0 = 1$.

2.4 Constitutive Equations. As energy is stored at the chain level, it is now possible to define a free energy density Ψ for the network. In each direction, we can predict the average stored elastic energy in a chain as $\psi(\lambda)$ with the energy functional of Eq. (1). The total energy of the network is then found by summing the contribution of each chain, which identifies in this approach as an integral over the unit sphere.

$$\Psi = \int_S \psi \rho dS + \pi(\det \mathbf{F} - 1) \tag{15}$$

where π is a Lagrange multiplier that enforces incompressibility. For the model to be thermodynamically consistent, we define the Cauchy stress σ to satisfy the Clausius–Duhem inequality, $\sigma : \mathbf{L} - \dot{\Psi} \geq 0$. Following the derivation in Appendix B, the Cauchy stress takes the form

$$\sigma = \sqrt{N} b \int_S f\lambda \rho (\mathbf{e}_r \otimes \mathbf{e}_r) dS + \pi \mathbf{I} \tag{16}$$

Constitutively, the elastic behavior of the TMM is similar to previous fully incompressible microsphere models [31,32]. We particularly note the similarity between Eq. (16) and the full network theory of Wu and Van der Geissen [44] and illustrate their equivalence for the limiting case of purely elastic chains in Sec. 3.2. The mechanical dissipation as a result of bond detachment also follows from the same derivation (Appendix B):

$$D = \int_S \xi_d \psi - \xi_a \psi_0 \, dS \geq 0 \tag{17}$$

Here, $\psi_0 = \psi(\lambda_0)$ is the average energy stored in a chain at its resting length. The dissipation has two clear contributions stemming from single chain kinetics. The first term is the energy dissipated by chains detaching from their stretched state, while the second term is the energy stored by attachment events. The dissipation equation thus states that the network cannot gain energy by attachment events—placing physical restrictions on the bond kinetics. Considering that the bond exchange in difference directions is independent, the dissipation equation imposes the following condition:

$$\xi_d \geq \xi_a \frac{\psi_0}{\psi} \tag{18}$$

For any positive and quadratic energy functional, $\psi \geq \psi_0$. This means that in an equilibrium state, Eq. (18) is always satisfied, as the rates of attachment and detachment are equal. Away from equilibrium, the functional form of the kinetic rates must however be chosen appropriately to satisfy the condition that the left-hand side grows faster than the right-hand side. This is ensured for any first-order kinetic equation, providing that k_d is either constant or monotonically increasing and k_a is either constant or monotonically decreasing. The kinetic model presented in this paper satisfies these requirements.

3 Model Predictions

The model presented in the previous section possesses a limited set of intrinsic variables as displayed in Table 1. In this section, we demonstrate that a large number of the reported properties of dynamic networks can be predicted using this limited set of physical parameters. We first briefly outline our discretization and solution procedure to provide a foundation for the illustrations to be presented. Following this, we compare the TMM to earlier hyperelastic and viscoelastic models. Finally, we outline the key findings of our study by identifying the response regimes exhibited by the model.

3.1 Discretization and Illustration. The finite domain of the microsphere facilitates a reduced numerical procedure without compromising the anisotropic properties of the network. To solve the differential equations presented in the previous section, we first discretize the microsphere on a 200×200 grid for $-\pi/2 \leq \theta \leq \pi/2$ and $0 \leq \varphi \leq \pi/2$, noting that symmetry allows us to only consider half of the unit sphere. With the initial conditions $\rho = \rho_0$ and $\mu = \mu_0$, we use a backward-Euler integration scheme to track the chain conformation given a specified velocity gradient $\mathbf{L}$. A typical iteration thus consists of (i) evolving ρ and μ at the current time, (ii) solving for the Cauchy stress and energy dissipation by trapezoidal integration, and (iii) determining ρ and $\dot{\mu}$ for the next time-step. We note here that, unless stated otherwise, the initial concentration of attached chains c_0 is maintained at 75% of the total population ($c_0 = 0.75 c_t$) and the chain length is kept at $N = 10$ for each illustration in this section. The Cauchy stress is normalized by the shear modulus $c_0 k_b T$ in all plots for generality.

For illustration purposes, we first provide examples of two experiments commonly used to measure viscoelasticity: stress relaxation and cyclic loading. For clarity, we introduce the Weissenberg number W, which describes the relative rates of elastic distortion and intrinsic relaxation. In this study, we define it as

$$W = |\mathbf{L}|/k_{d,0} \tag{19}$$

where $|\mathbf{L}|$ is the spectral norm of the velocity gradient $\mathbf{L}$. For low W ($W \ll 1$), the bond dynamics overwhelm the elastic distortion, and the network flows as a fluid. Conversely, for large W ($W \gg 1$), the chains do not have time to detach during loading, and the network behaves elastically. These limiting cases are discussed further in Sec. 3.2.

To demonstrate some of the simple predictions of the TMM, we first investigate the response of a single network consisting of bonds that detach according to Eq. (11) and reattach at a constant rate k_a. We take f_0 to be very large ($f_0 > 100$), so that the detachment rate is approximately constant for small loadings (Fig. 1(b)). The network is subjected to simple shear in the x_1 direction at a rate much greater

Table 1 Model parameters

Parameter	Description	Units
c_t	Total chain density	Chains/volume
N	Chain length	Kuhn segments
b	Kuhn segment length	Length
k_d	Detachment rate	Chains/second
k_a	Attachment rate	Chains/second
f_0	Chain sensitivity	Force

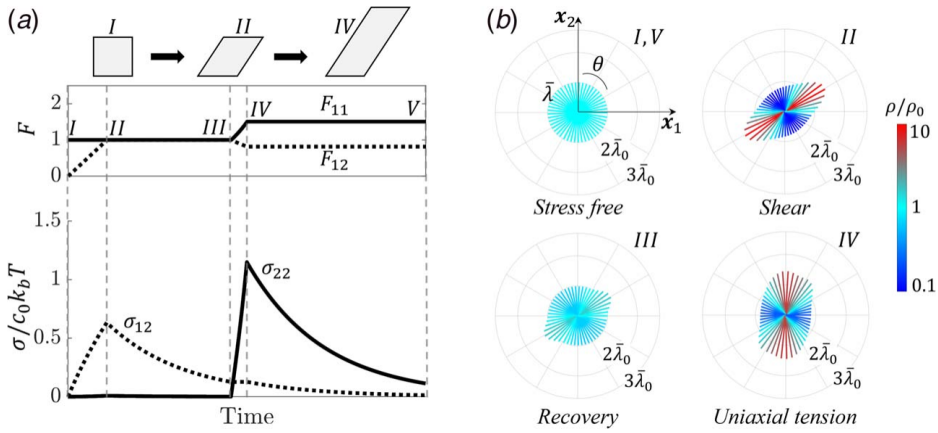

Fig. 3 Simple illustration of a stretch-hold simulation in shear followed by uniaxial tension. (a) Predicted stress response (Cauchy stress) of the TMM. Roman numerals I–V correspond to respective portions of the loading curve (inset). (b) Polar plots of λ as a function of azimuthal angle θ, taken as a "slice" of the surface on the x – y plane. Lines are colored by their directional chain density ρ.

than its resting kinetics (W = 100). We load to a shear of $F_{12} = 1$, hold at for a short period of time before loading in uniaxial tension at the same Weissenberg number to $F_{11} = 1.5$, and then hold at this stretch indefinitely (Fig. 3(a)). The decrease in F_{12} during the uniaxial loading phase is due to the incompressibility of the material (requiring det F = 1). The corresponding stress versus time curve displays nonlinear stiffening behavior in the loading regimes (I–II and III–IV) and Maxwellian relaxation in the hold regimes (II–III and IV–V).

To illustrate the microstructural evolution predicted by the TMM, we plot in Fig. 3(b) the directional density ρ and average chain stretch λ within the plane of loading (φ = π/2 for uniaxial tension in the x_1 direction). Here, the length of each line in a direction θ corresponds to the average chain stretch λ, while the color is mapped to the directional chain density ρ in that direction. The top-left panel shows that the network is initially isotropic, as each line is the same length and color. During loading, the model predicts an increase in both the average stretch and density of chains in the principal loading direction (θ = π/4). A partial recovery is observed at time III, which is due to chain detachment from their stretched state and reattachment in their initial configuration. The network maintains a small amount of shear when loading in uniaxial tension as observed in panel IV. We predict full stress relaxation in the limit of $t \to \infty$, as indicated by the V in the top-left panel. The illustrations depicted in Fig. 3(b) will be used for the remainder of the paper, but the scale and colorbars will be omitted to avoid crowding the figures. All future illustrations maintain the same scale system established in this figure.

3.2 Limiting Cases and Convergence to Earlier Models. The behavior of physical networks can exhibit a range of responses from that of elastic solids at high strain rates (W ⪢ 1), to that of viscous fluids at low rates (W ⪡ 1) [20]. In the context of the proposed model, the limit of large f_0 ($f_0 \to \infty$) corresponds to regimes where bond dynamics are independent of force (k_d remains constant). The time dependence of the network is therefore fully decoupled from its deformation history. In these conditions, we compare the predictions of the TMM to earlier formulations under cyclic loading conditions and at various rates.

Elastic response. If the rate of loading is large (W ⪢ 1), chains do not have time to detach during loading, and the network behaves elastically. There is no energy dissipation, and the curves in their loading and unloading regimes look identical (Fig. 4(a)). The TMM predicts severe strain stiffening around $\lambda = 1/\sqrt{N}$ as chains align and reach their contour length along the loading direction. In fact, at high strain rates, the TMM converges to the elastic microsphere models originally proposed by Treloar [43,46], for which generalized solutions were derived by Wu and Van der Giessen [29,44]. Thus, the TMM may be thought of as an extension of these earlier models with incorporated chain kinetics. The microsphere formulation predicts more stiffening than isotropic stretch

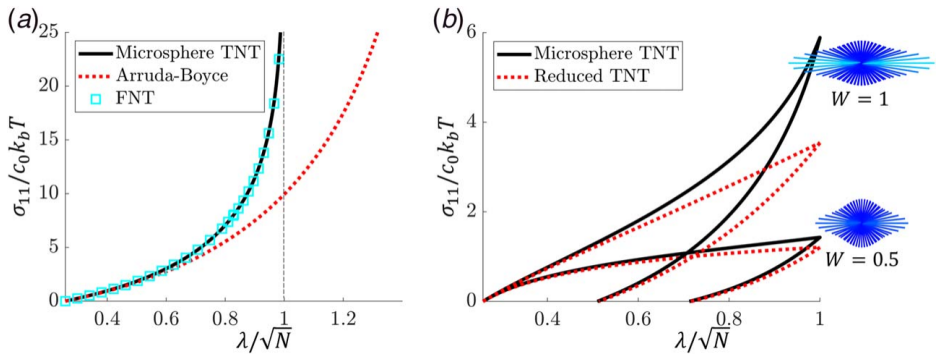

Fig. 4 Limiting cases of the TMM. (a) Uniaxial tension at a high loading rate (W = 100). The model converges to the Full Network Theory (FNT) of Wu and Van der Giessen. (b) Cyclic loading at small strain rates. The TMM predicts a more nonlinear curve than previous (reduced) models [21] due to the anisotropic stretch measure λ. Polar plots are displayed at the peak of loading for each simulation.

models, such as the eight-chains model of Arruda and Boyce [28], which average the chain-stretch over all directions. It is worth noting that isotropic stretch models have actually been shown to outperform Microsphere formulations under certain loading conditions (for instance, when considering both uniaxial and biaxial response simultaneously). This point is further addressed in Sec. 4.

Linear viscoelastic response. Let us now investigate the prediction of the TMM for constant bond dynamics, but moderate to low strain rates (i.e., $W \leq 1$). In these regimes, the network exhibits a combination of creep and elasticity that can be measured by hysteresis loops during cyclic loading. As shown in Fig. 4(b), the form of the stress-strain curve depends heavily on the loading rate. Previous models for capturing the effects of nonlinear elasticity and constant bond dynamics include the reduced transient network theory [37]. In this earlier formulation, the average elastic deformation of the chain was described by the conformation tensor μ, which is allowed to relax over time at rate k_d. Using an Arruda-Boyce like approximation for the network elasticity, the model predicted hysteresis loops shown as dotted lines in Fig. 4(b). The predictions of the TMM show notable discrepancies to the reduced transient network theory when the strain rate is large ($W = 1$ in the figure), but a convergence at very low strain rates ($W = 0.5$ in the figure). Similar to the elastic comparisons of Fig. 4(a), we observe that the TMM predicts more stiffening of the network at larger strains, and this effect becomes predominant as the strain rate increases. This observation can be explained by the degree of anisotropy developed in elastic networks; at high loading rates, chains tend to align and deform elastically in the stretch directions, thereby inducing a large proportion of highly stretched chains along the principal axis. This phenomenon, responsible for network stiffening, is not well-captured by the "average" tensorial form of the reduced Transient Network Theory. At low strain rates however, chains have time to detach from the network before becoming severely deformed. The network therefore remains more isotropic, with less elastic deformation—a regime that can be captured by an average tensorial formulation. To summarize, the TMM better reflects the anisotropic properties of the network either for elastic networks or at higher loading rates ($W \geq 0.5$).

3.3 The Role of Force Sensitivity. Let us now explore the role of the bonds' force sensitivity on the mechanical response of the network. For this, we once again consider a cyclic loading scenario where the network is first deformed to a stretch $\lambda = \sqrt{N}$, after which it is immediately returned to its initial state at the same rate. To gain further insight into the microstructure, we follow the evolution of the density c of attached chains (see Eq. (8)), as well as the average directional stretch and chain density in the loading direction, defined by

$$\bar{\lambda} = \lambda(\theta_p, \varphi_p), \quad \rho_p = \rho(\theta_p, \varphi_p)/\rho_0$$

Here, φ_p and θ_p are, respectively, the polar and azimuthal angles defining vector $\mathbf{x}_1$. Note that ρ_p is normalized by its initial value for convenience.

To set a reference, we first show in Fig. 5, the stress response of a network with constant bond dynamics ($f_0 \to \infty$) at varying loading rates. It can be shown that when bond dynamics are decoupled from mechanics, the overall chain concentration remains constant and equal to its base value c_0 (determined in Eq. (13)) regardless of deformation history. In this case, the viscoelastic response—which is due to bond exchange only, but with no change in chain concentration—exhibits a stiffening regime that becomes less and less noticeable as W decreases. This is accompanied with an increase in viscous dissipation (due to bond exchange) that can visually be observed by the area enclosed within the hysteresis loops in Fig. 5. For these networks, the TMM predicts that the evolution of the local chain stretch λ_p and density ρ_p closely follow their macroscopic counterparts; the directional stretch linearly increases with the macroscopic deformation, while the directional density (or chain alignment) exhibits similar hysteresis loop as the Cauchy stress. This second trend results from a lag in the chain alignment (compared to the applied strain) due to bond dynamics.

To illustrate the effect of force-sensitive bond detachment, let us now consider the fastest loading rate ($W = 10$) in Fig. 5 and explore the network response as f_0 varies from 1 to 10 (Fig. 6). For the largest value of f_0, a similar curve is recovered, with very little hysteresis loop. As bond kinetics become more sensitive to force, however, a clear trend of softening is observed, with a more pronounced hysteresis. This is explained by considering the increasing number of highly stretched chains with deformation; as this number increases, detachment events begin to overwhelm reattachment events due to accelerated bond kinetics. Indeed, the induced drop in the total concentration of attached chains, c, is most prevalent for the most sensitive chains (lowest f_0). We note that the change in c is a temporary consequence of the deformation and the TMM predicts full recovery of the chain concentration after unloading. The mechanisms by which chains stretch and detach are readily observed in the evolution of the directional stretch λ_p and chain density ρ_p. We see here that at low deformations, the chains tend to realign with stretch, but this realignment is accompanied with a fast detachment of the most elongated chains. As the second mechanism prevails, we observe a drop in both the density of chains along the principal axis and their average stretch. These events together are responsible for the noticeable stress softening at the network level. As expected, this softening initiates earlier if the force sensitivity of the bond is large (i.e., f_0 is low). Thus, the chain sensitivity can be an important factor in activating energy dissipation, as observed by the increasing area within the hysteresis loop for lower f_0. This dissipation mechanism is however quite different from the networks with constant bond kinetics presented in Fig. 5, and this difference can be observed in the distinct signature of the stress-strain curves. In real polymers, energy dissipation may

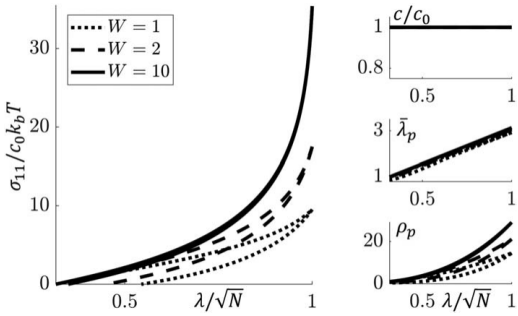

Fig. 5 Cyclic loading experiment in uniaxial tension for a network with constant k_d (high f_0) at varying Weissenberg numbers

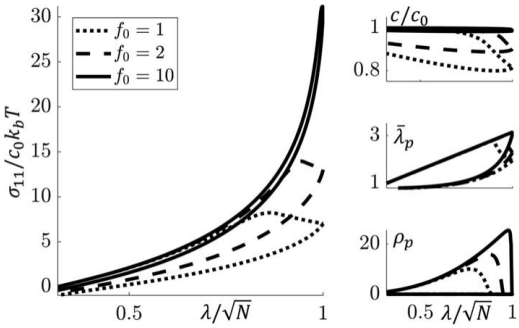

Fig. 6 Cyclic loading experiment in uniaxial tension at $W = 10$ for networks with varying f_0

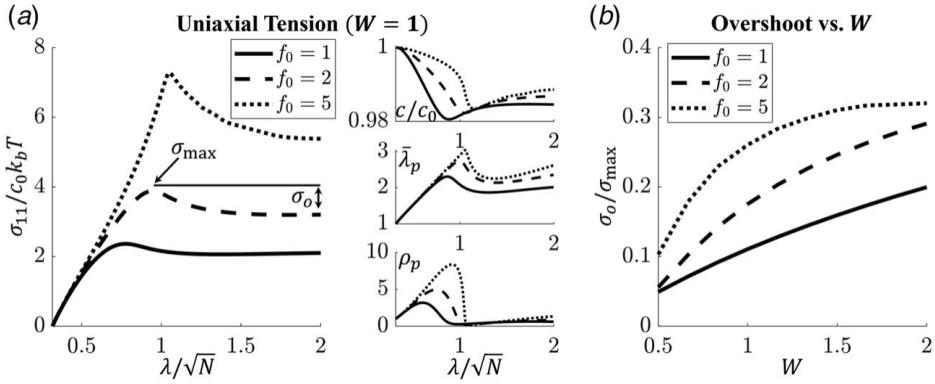

Fig. 7 (a) Uniaxial tension at W = 1 with varying f_0. The stress overshoot σ_0 is defined as the difference between the peak stress σ_{max} and the steady-state stress. (b) The relative overshoot σ_0/σ_{max} as a function of f_0 and W.

arise from a combination of these two processes, yielding more complex responses discussed in the next section.

3.4 Elasticity, Flow, and Rupture of Transient Networks. We here present a detailed study of the TMM by considering the deformation of a network at a constant loading rate. Three dynamic processes govern the response of the network: (i) the elastic distortion of attached chains, (ii) the accelerated detachment of highly stretched chains, and (iii) the realignment of chains in the direction of loading. Each of these processes are coupled with each other: elastic deformation induces a faster detachment rate of highly stretched chains, chain alignment creates a higher concentration of chains detaching at a faster rate, and the reattachment of chains in their stress-free state temporarily resets the process in all directions for each increment of deformation. The evolution of the network thus consists of a transient regime, during which these processes equilibrate with the constant loading rate, and an equilibrium state, at which point the network topology has reached a state of dynamic equilibrium. The duration and difference between these two regimes are determined by the Weissenberg number W and the bond sensitivity f_0. In this section, we demonstrate a large variety of responses that can be captured by different combinations of these two parameters.

As the system equilibrates with loading, we expect the stress response to closely reflect the evolution of the microstructure. Indeed, the stress response predicted by the TMM typically consists of an initially increasing regime, followed by a creeping flow at large deformations. In Fig. 7(a), we illustrate the uniaxial tension response predicted by the TMM for networks with $f_0 = 1$, $f_0 = 2$, and $f_0 = 5$ at a loading rate of W = 1. In each case, a noticeable stress overshoot is observed, which marks the transition from the transient response to the equilibrium state. Increasing f_0 delays the acceleration of bond kinetics, creating a longer transient regime and a larger stress overshoot. We see that the point of overshoot corresponds with a sudden drop in ρ_p and λ_p, which indicates the existence of a critical stretch at which point the detachment rate of highly aligned chains overwhelms the loading rate. Indeed, the peak value of λ_p increases with increasing f_0, and the drop in ρ_p becomes steeper. The secondary rise in λ_p and ρ_p is due to the stretching and alignment of fresh chains that have reattached to the network in a stress-free state after a detachment event. Figure 7(b) summarizes the stress overshoot predicted by the TMM as a function of W and f_0. Here, we normalize the overshoot σ_o by the corresponding peak stress σ_{max} to promote an easier comparison. As expected, the lowest value of f_0 achieves the smallest relative overshoot, as the detachment rate of chains accelerates very quickly for this network. Increasing the Weissenberg number further delays yielding as elastic deformation is more influential. This creates a longer transient regime with a larger stress overshoot.

As we further increase the Weissenberg number, chains do not have time to detach from the network during loading, and there is a buildup of highly stretched chains. From Fig. 7, we expect this to be accompanied by a more delayed and extreme stress overshoot. In Fig. 8, we illustrate the same range of f_0 values as before, but at a higher Weissenberg number of W = 10. For small stretches, loading at this rate is fast enough to maintain a nearly elastic response, and each curve follows the same stiffening behavior. Once again, yielding coincides with a sudden decrease in ρ_p and λ_p, but this time, we also observe a markable drop in the total chain concentration c/c_0.

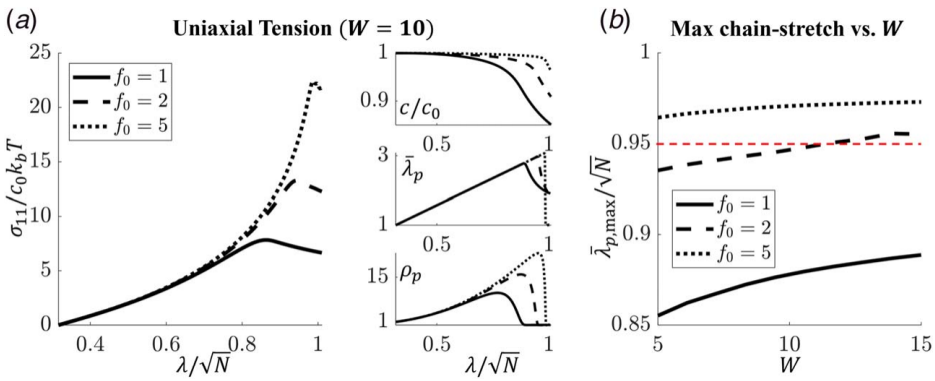

Fig. 8 (a) Uniaxial tension at W = 10 with varying f_0. (b) The maximum chain-level stretch λ_p as a function of f_0 and W in the fast-loading regime. The dashed horizontal line indicates stretching a chain to 95% of its contour length.

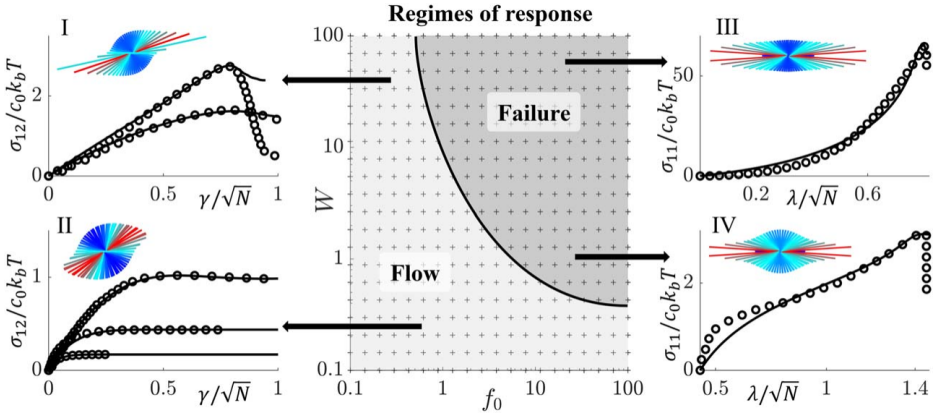

Fig. 9 Phase diagram of the stable and unstable regions predicted by the TMM. Experimental data are denoted with black circles and are taken from Refs. [3] (I: top-left), [14] (II: bottom-left), [6] (III: top-right), and [49] (IV: bottom-right). Polar plots indicate the equilibrium (final) distribution for the given simulation.

This is explained by the higher degree of alignment at this loading rate; very few chains have detached during deformation, so the detachment event consists of a larger population of chains that have been stretched since the onset of loading. Once again, increasing f_0 delays the yielding and creates a higher peak stress.

At such large values of W, the stretch felt by chains prior to yielding increases significantly, and at a certain point, chain rupture is preferred over reversible bond detachment. Depending on the value of f_0, the maximum chain-level stretch λ_p could approach 95%–99% of the contour length $\ell = Nb$ (Fig. 8(b)). At this level of deformation, the bond angle of the backbone chain itself is stretched, which is closely followed by chain scission [47]. By following the stretch felt by a chain in a given direction, the TMM provides an estimate to predict chain rupture and the onset of damage. For this purpose, we use a generic rupture criterion based on the maximum directional chain stretch λ_p. We postulate that failure occurs when:

$$\lambda_p = 0.95\sqrt{N}$$

which corresponds to a situation where a chain is stretched to 95% of its contour length (illustrated by the dashed red line in Fig. 8(b)). Using this criterion, we performed 400 simulations that spanned the parameter space $\{W, f_0\}$ and identified two main regimes in the stress-strain signature of the network (Fig. 9). The first is identified as the flow regime, where the strain rate is either low enough, or the bond dynamics sensitive enough to favor flow over rupture. The second is denoted as the failure regime, which exists for higher strain rates and lower force sensitivity of the bond. In this regime, chains are eventually stretched above λ_p and rupture, which marks the end of the simulation.

This parametric study of the TMM reveals a large number of characteristic responses, which can potentially be used to physically interpret the behavior of previously studied physical networks. For instance, the fluid-like creep of associative polymer solutions is well-approximated by the TMM in the flow regime (left plots of Fig. 9). The bottom-left plot shows excellent agreement with shear startup experiments performed by Berret and Séréro [1,14] in the shear-thinning regime of their telechelic associative polymer solutions. Each curve reflects shear at a different loading rate, which varied between $W = 0.2$ and $W = 1.8$, with the highest stress being achieved at the highest loading rate. For this material, we determined a fitted value of f_0 (see Table 2I) based on the length scale of the backbone polyethylene oxide (PEO) [14]. We particularly note that the TMM accurately predicts both the transient and equilibrium response of the network. In contrast, the TMM underpredicts the stress overshoot observed in the faster experiments ($2.5 \le W \le 5$) done by Skrzeszewka et al. [36] for a similar family of telechelic polymers (top-left plot in Fig. 9). A larger overshoot induces a stress softening response that is known to be associated with strain localization. In this context, a higher loading rate induces the onset of shear banding within the material [1], which cannot be predicted by a local continuum model [48]. The polymers studied by Skrzeszewka et al. had a more complex collagen-like structure [3,36], which makes the determination of the Kuhn length b less well-defined. The normalized value of f_0 is, therefore, presented in Table 2 (II).

The failure regime of the TMM consists of two distinct responses characterized by the rate of loading. If the loading is moderate ($W \approx 1$), the model predicts a response similar to unsteady creep; the stress initially softens due to the low loading rate, but begins to stiffen at higher stretches as some chains approach their nonlinear regime. This is therefore only observed for bonds with high f_0. The corresponding "S"-shaped curve was observed from the ionically bonded triblock copolymers studied by Henderson et al. [49] (bottom-right plot in Fig. 9). This network was similar in composition to the associative solutions studied previously, but the ionically modified end-groups creates an even more robustly connected network. Based on the length scale of the middle-group, poly(methacrylic acid) (PMAA), we fitted f_0 with a loading rate of $W = 1.35$ (Table 2(III)). It is interesting to note that the predictions of the TMM in this regime match closely with the rubbery viscoelasticity microsphere model of Miehe and Göktepe [34]. In this light, the dynamics of reptation and the release of entanglements in elastomers could be interpreted as the detachment of physical bonds between neighboring polymer chains. At larger Weissenberg numbers ($W \ge 10$), the model predicts a purely stiffening response as discussed in Sec. 3.2. This type of rubber-like response was observed in the supramolecular network of Cordier et al. [6] (top-right plot in Fig. 9). The network consisted of a robust hydrogen-bonding network of multitopic molecules, which can be interpreted as scattered chains of clustered molecules held together by weak interactions. These clusters can be represented as freely jointed

Table 2 Fitted model parameters

Parameter	I—Ref. [3]	II—Ref. [14]	III—Ref. [6]	IV—Ref. [49]
c_t	7.0×10^{21} m^{-3}	1.6×10^{22} m^{-3}	7.9×10^{18} m^{-3}	7.8×10^{20} m^{-3}
N	270	78	230	13
b	N/A	0.8 nm	N/A	1.3 nm
k_d	0.42 s^{-1}	1.8 s^{-1}	0.38 s^{-1}	2.9 s^{-1}
k_a	7.9 s^{-1}	34 s^{-1}	0.02 s^{-1}	54.3 s^{-1}
f_0	2.5 k_bT/b	3.7 pN	3.0 k_bT/b	57 pN

chains if there are minimal interactions between neighboring units on the same chain. The stiffening behavior and point of failure is well-captured by the TMM. We use a normalized value of f_0 for fitting (Table 2 (IV)) given the unorthodox chain topology.

4 Conclusion and Discussion

In this study, we presented the transient microsphere model (TMM)—a microsphere formulation of the Transient Network Theory—to explore the role of force-sensitive bond kinetics in physical networks. The elastic response at high loading rates was compared to previous hyperelastic models, such as the full network theory of Wu and Van der Geissen, which the TMM converges to in the limit of large Weissenberg number. We also compared the TMM to previous reductions of the transient network theory and demonstrated a higher degree of stiffening, which is not well-approximated by the average stretch at large deformations. Upon incorporating force sensitivity into the bond kinetics, we observed two sources of energy dissipation in physical networks: (i) bond exchange without losses in the total chain concentration and (ii) network softening due to force-accelerated bond exchange. These processes yielded distinct regimes of response for simple loading scenarios such as uniaxial tension and simple shear, which were dependent on the rate of loading (W) and the bond sensitivity (f_0). When chain kinetics dominated the response of the material (low W and low f_0), the TMM predicts a stable stress-strain curve that ends in steady-state creep. If the material deforms more elastically (high W and high f_0), localized directions of sudden detachment events offered a metric for predicting failure. Using published experimental data, we demonstrated that each regime predicted by the model has been observed in physical polymer networks of varying composition. The TMM could therefore be used to quantify these networks based on physical parameters such as their rate of detachment and bond strength.

The presented model rests on several assumptions which could be broadened depending on the system being studied. In particular, it is known that the affine assumption breaks down at large deformations. As we are mainly interested in the viscoelastic properties of the network, we maintain the affine assumption and note that non-affine characteristics could be added later. We also note here that our formulation is only instantaneously affine with the macroscopic velocity gradient (hence, we write $\dot{\mathbf{r}} = \mathbf{L}\mathbf{r}$). Due to bond kinetics, the stretch felt by an individual chain does not reflect the global deformation gradient $\mathbf{F}$ except for the purely elastic case ($W \to \infty$). Other characteristics of non-affine behavior have further been accounted for in a microsphere model by Miehe et al. [30]. It is also interesting to note that the stiffening behavior of rubbers is better approximated by the seemingly less-precise Arruda–Boyce model, which uses an isotropic approximation for the chain stretch [50]. The divergence of materials from their predicted alignment is likely also due to non-affine behaviors and topological constraints such as entanglements [30]. We believe that the added precision in modeling the anisotropic viscoelastic response sufficiently makes up for the loss of precision in this one regime.

A clear advantage to the microsphere approach is a finite numerical domain that still accounts for directional properties. Previous microsphere models [30,32] have further reduced their computational domain by using quadrature schemes such as those presented by Bazant and Oh [51]. This allows for the incorporation of fully anisotropic constitutive laws into more sophisticated studies using the finite element method [30]. This remains possible with the TMM, but the spatial derivatives in Eqs. (9) and (10) would be challenging to compute on a discrete quadrature grid. Future implementations of this model could surpass this by using an embedded finite element method such as Arbitrary Lagrangian–Eulerian, which uses an Eulerian material description in combination with a moving Lagrangian mesh. This model could then be used to predict more complex material processes such as fracture.

Physically bonded networks have been getting increased attention for their ability to strengthen materials via sacrificial bonding [7]. The desire to understand physical networks alone is thus vital to their success, but combining networks into hybrid materials is a primary application. Many methods of modeling these hybrid networks have been proposed, which could incorporate the effects of polydispersity [33] and various network interactions [30]. We note that it is possible to qualitatively predict these behaviors by summing networks in parallel (equal strain assumption) [21]. This could be done with the TMM to model hybrid materials with constituent networks ranging anywhere from purely elastic to linearly viscoelastic. On this note, the TMM, as presented in this work, is restricted to describing one characteristic timescale of a given network (determined by the rate $k_{d,0}$). Many real physical networks are however known to be better represented by a spectrum of timescales. These aspects may be easily incorporated into the TMM by considering multiple networks in parallel as discussed in prior works [20], an approach that is akin to a prony series decomposition. Another interesting feature of weak bonding interactions is their tendency to form clusters or a strong junction consisting of many weak interactions. The strength of these junctions varies depending on the number of contributing bonds [52]. This induces complex viscoelastic behaviors such as yielding and stress overshoot, which the TMM captures with the force sensitivity f_0. The added strength of a cluster of weak bonds can, therefore, be explained by a delayed acceleration of bond kinetics. From these observations, we believe that the insight provided by the TMM will be valuable for the rational design of materials for a desired function.

Acknowledgment

FJV gratefully acknowledges the support of the National Science Foundation under Award No. 1761918. The content is solely the responsibility of the authors and does not necessarily represent the official views of the National Science Foundation.

Conflict of Interest

There are no conflicts of interest.

Data Availability Statement

The authors attest that all data for this study are included in the paper.

Appendix A: Evolution Equations Derivation

In previous works, we have presented a Fokker–Planck equation for the probability density function $\Phi = c(t)P(r, \theta, \varphi)$ [20]. For convenience, we write it here:

$$\frac{d\Phi}{dt} = -\mathbf{L} : \left[\frac{\partial \Phi}{\partial \mathbf{r}} \otimes \mathbf{r}\right] + k_a(c_t - c)P_0 - k_d\Phi \tag{A1}$$

We note the same terms reflecting the elastic distortion of the network and viscous dissipation due to bond detachment. It is also important to note that this equation is derived with the incompressibility assumption ($\mathrm{Tr}\,\mathbf{L} = 0$). We will begin from here to reduce this equation to its micro-sphere counterparts in Eqs. (9) and (10). We first note the expansion of the divergence a scalar field f into spherical coordinates as

$$\nabla f = \frac{\partial f}{\partial r}\mathbf{e}_r + \frac{1}{r\sin\varphi}\frac{\partial f}{\partial \theta}\mathbf{e}_\theta + \frac{1}{r}\frac{\partial f}{\partial \varphi}\mathbf{e}_\varphi \tag{A2}$$

Using index notation will be convenient for further derivations, so we will change our notation for the spherical basis vectors as $\hat{\mathbf{r}}_i$, $\hat{\boldsymbol{\theta}}_i$, and $\hat{\boldsymbol{\varphi}}_i$. The elastic distortion of the network comprises the bulk of

this derivation, so we will consider here a network whose detachment rates are both zero ($k_d = k_a = 0$). In this case, the differential Eq. (A1) is written

$$\frac{\partial \Phi}{\partial t} = -L_{ij} \frac{\partial \Phi}{\partial r_i} r_j = -L_{ij} \hat{r}_j \left(r \frac{\partial \Phi}{\partial r} \hat{r}_i + \frac{1}{\sin\varphi} \frac{\partial \Phi}{\partial \theta} \hat{\theta}_i + \frac{\partial \Phi}{\partial \varphi} \hat{\varphi}_i \right) \tag{A3}$$

To derive Eq. (9), we multiply by r^2 and integrate in the radial direction,

$$\begin{aligned} \int_0^\infty \frac{\partial \Phi}{\partial t} r^2 dr &= -L_{ij} \hat{r}_j \left(\int_0^\infty r^3 \frac{\partial \Phi}{\partial r} \hat{r}_i + \int_0^\infty r^2 \frac{\partial \Phi}{\partial \theta} \hat{\theta}_i + \int_0^\infty r^2 \frac{\partial \Phi}{\partial \varphi} \hat{\varphi}_i dr \right) \\ &= -L_{ij} \hat{r}_j \left(\hat{r}_i \int_0^\infty r^3 \frac{\partial \Phi}{\partial r} dr + \frac{\hat{\theta}_i}{\sin\varphi} \int_0^\infty r^2 \frac{\partial \Phi}{\partial \theta} dr + \hat{\varphi}_i \int_0^\infty r^2 \frac{\partial \Phi}{\partial \varphi} dr \right) \\ &= L_{ij} \hat{r}_j \left(\hat{r}_i \int_0^\infty \Phi \frac{\partial}{\partial r} r^3 dr + \frac{\hat{\theta}_i}{\sin\varphi} \frac{\partial}{\partial \theta} \int_0^\infty \Phi r^2 dr + \varphi_i \frac{\partial}{\partial \varphi} \int_0^\infty \Phi r^2 dr \right) \\ &= L_{ij} \hat{r}_j \left(3 \hat{r}_i \rho + \frac{\hat{\theta}_i}{\sin\varphi} \frac{\partial \rho}{\partial \theta} + \hat{\varphi}_i \frac{\partial \rho}{\partial \varphi} \right) \end{aligned} \tag{A4}$$

Integration by parts was used on each term, and it is easy to see that boundary terms vanish for all cases. The addition of attachment and detachment terms does not increase the complexity of the derivation, and the evolution of μ is found by a similar method.

Appendix B: Deriving the Cauchy Stress and Energy Dissipation

In the absence of thermal fluctuations and changes in volume, the Clausius–Duhem inequality is written per unit volume as

$$\mathsf{D} = \sigma : L - \dot{\Psi} \geq 0 \tag{B1}$$

where D is the energy dissipation per unit volume. Using the definition in Eq. (15), the material derivative of the macroscopic energy Ψ is

$$\frac{D\Psi}{Dt} = \int_S \rho \frac{D\psi}{Dt} dS + \int_S \psi \frac{D\rho}{Dt} dS \tag{B2}$$

where $D(\cdot)/Dt$ denotes the material derivative, whose form is given for an arbitrary function f of θ and φ as

$$\frac{Df(\theta,\varphi)}{Dt} = \frac{\partial f}{\partial t} + L : (e_r \cdot \nabla f) \tag{B3}$$

We note that this definition depends on our Eulerian definition of the unit sphere S and the radial coordinate r is equal to unity. The bulk of this section thus relies on deriving an expression for the material time derivative of the chain-level stored elastic energy ψ. We first note the following use of the chain rule:

$$\frac{D\psi}{Dt} = \frac{\partial \psi}{\partial \lambda} \frac{D\lambda}{Dt} = f \sqrt{N b} \frac{D\lambda}{Dt} \tag{B4}$$

The time derivative of λ is defined using the chain rule,

$$\frac{\partial \lambda}{\partial t} = \frac{1}{2\lambda} \left(\frac{1}{\mu} \frac{\partial \mu}{\partial t} - \frac{1}{\rho} \frac{\partial \rho}{\partial t} \right) \tag{B5}$$

A simple application of Eqs. (9) and (10) yields

$$\frac{\partial \lambda}{\partial t} = L : \left(\lambda e_r \otimes e_r - \frac{1}{\sin\varphi} \frac{\partial \lambda}{\partial \theta} e_\theta \otimes e_r - \frac{\partial \lambda}{\partial \varphi} e_\varphi \otimes e_r \right) + k_a \left(\frac{c_t}{\sqrt{\mu_0 / \rho_0}} - 1 \right) \sqrt{\mu \rho} \tag{B6}$$

Combining this with the divergence term yields a simple evolution law for the average stretch,

$$\frac{D\lambda}{Dt} = \lambda (L : e_r \otimes e_r) \tag{B7}$$

We can now write the material time derivative of the chain-level stored elastic energy as

$$\frac{D\psi}{Dt} = f \sqrt{N b} \lambda (L : e_r \otimes e_r) \tag{B8}$$

Putting this into the expression for the Clausius–Duhem inequality,

$$D = \sigma : L - \rho f \sqrt{N b} \lambda (L : e_r \otimes e_r) dS - \int_S [k_a \rho_0 (c_t/c - 1) - k_d \rho] \psi \, dS \geq 0 \tag{B9}$$

Rearranging and reordering terms, the Cauchy stress and energy dissipation of Eqs. (16) and (17) are recovered.

References

[1] Berret, J.-F., and Séréro, Y., 2001, "Evidence of Shear-Induced Fluid Fracture in Telechelic Polymer Networks," Phys. Rev. Lett., 87(4), p. 048303.
[2] Erk, K. A., and Shull, K. R., 2011, "Rate-Dependent Stiffening and Strain Localization in Physically Associating Solutions," Macromolecules, 44(4), pp. 932–939.
[3] Skrzeszewska, P. J., Wolf, F. A. d., Werten, M. W. T., Moers, A. P. H. A., Stuart, M. A. C., and Gucht, J. v. d., 2009, "Physical Gels of Telechelic Triblock Copolymers With Precisely Defined Junction Multiplicity," Soft Matter, 5(10), pp. 2057–2062.
[4] Thornell, T. L., Helfrecht, B. A., Mullen, S. A., Bawiskar, A., and Erk, K. A., 2014, "Fracture-Healing Kinetics of Thermoreversible Physical Gels Quantified by Shear Rheophysical Experiments," ACS Macro Lett., 3(10), pp. 1069–1073.
[5] Yan, T., Schröter, K., Herbst, F., Binder, W. H., and Thurn-Albrecht, T., 2016, "Unveiling the Molecular Mechanism of Self-Healing in a Telechelic, Supramolecular Polymer Network," Sci. Rep., 6(1), p. 32356.
[6] Cordier, P., Tournilhac, F., Soulié-Ziakovic, C., and Leibler, L., 2008, "Self-Healing and Thermoreversible Rubber From Supramolecular Assembly," Nature, 451(7181), pp. 977–980.
[7] Creton, C., and Ciccotti, M., 2016, "Fracture and Adhesion of Soft Materials: A Review," Rep. Prog. Phys., 79(4), p. 046601.
[8] Eyring, H., 1935, "The Activated Complex in Chemical Reactions," J. Chem. Phys., 3(2), pp. 107–115.
[9] Kramers, H. A., 1940, "Brownian Motion in a Field of Force and the Diffusion Model of Chemical Reactions," Physica, 7(4), pp. 284–304.
[10] Annable, T., Buscall, R., Ettelaie, R., and Whittlestone, D., 1993, "The Rheology of Solutions of Associating Polymers: Comparison of Experimental Behavior With Transient Network Theory," J. Rheol., 37(4), pp. 695–726.
[11] Tanaka, F., and Edwards, S. F., 1992, "Viscoelastic Properties of Physically Crosslinked Networks. 1. Transient Network Theory," Macromolecules, 25(5), pp. 1516–1523.
[12] Erk, K. A., Henderson, K. J., and Shull, K. R., 2010, "Strain Stiffening in Synthetic and Biopolymer Networks," Biomacromolecules, 11(5), pp. 1358–1363.
[13] Erk, K. A., Martin, J. D., Hu, Y. T., and Shull, K. R., 2012, "Extreme Strain Localization and Sliding Friction in Physically Associating Polymer Gels," Langmuir, 28(9), pp. 4472–4478.
[14] Berret, J.-F., Séréro, Y., Winkelman, B., Calvet, D., Collet, A., and Viguier, M., 2001, "Nonlinear Rheology of Telechelic Polymer Networks," J. Rheol., 45(2), pp. 477–492.
[15] Werten, M. W. T., Teles, H., Moers, A. P. H. A., Wolbert, E. J. H., Sprakel, J., Eggink, G., and de Wolf, F. A., 2009, "Precision Gels From Collagen-Inspired Triblock Copolymers," Biomacromolecules, 10(5), pp. 1106–1113.
[16] Tam, K. C., Jenkins, R. D., Winnik, M. A., and Bassett, D. R., 1998, "A Structural Model of Hydrophobically Modified Urethane-Ethoxylate (HEUR) Associative Polymers in Shear Flows," Macromolecules, 31(13), pp. 4149–4159.
[17] Pham, Q. T., Russel, W. B., Thibeault, J. C., and Lau, W., 1999, "Micellar Solutions of Associative Triblock Copolymers: The Relationship Between Structure and Rheology," Macromolecules, 32(15), pp. 5139–5146.

[18] Yang, L., Tan, X., Wang, Z., and Zhang, X., 2015, "Supramolecular Polymers: Historical Development, Preparation, Characterization, and Functions," Chem. Rev., 115(15), pp. 7196–7239.
[19] Tanaka, F., and Edwards, S. F., 1992, "Viscoelastic Properties of Physically Crosslinked Networks: Part 1. Non-Linear Stationary Viscoelasticity," J. Non-Newtonian Fluid Mech., 43(2), pp. 247–271.
[20] Vernerey, F. J., Long, R., and Brighenti, R., 2017, "A Statistically-Based Continuum Theory for Polymers With Transient Networks," J. Mech. Phys. Solids, 107, pp. 1–20.
[21] Vernerey, F. J., Brighenti, R., Long, R., and Shen, T., 2018, "Statistical Damage Mechanics of Polymer Networks," Macromolecules, 51(17), pp. 6609–6622.
[22] Vernerey, F. J., Shen, T., Sridhar, S. L., and Wagner, R. J., 2018, "How Do Fire Ants Control the Rheology of Their Aggregations? A Statistical Mechanics Approach," J. R. Soc. Interface, 15(147), p. 20180642.
[23] Lalitha Sridhar, S., and Vernerey, F. J., 2018, "The Chain Distribution Tensor: Linking Nonlinear Rheology and Chain Anisotropy in Transient Polymers," Polymers, 10(8), p. 848.
[24] Lalitha Sridhar, S., Ortega, J. K., and Vernerey, F. J., 2018, "A Statistical Model of Expansive Growth in Plant and Fungal Cells: The Case of Phycomyces," Biophys. J., 115(12), pp. 2428–2442.
[25] Shen, T., and Vernerey, F. J., 2020, "Rate-Dependent Fracture in Transient Networks," J. Mech. Phys. Solids, 143, p. 104028.
[26] Vernerey, F. J., and Lamont, S., 2021, "Transient Mechanics of Slide-Ring Networks: A Continuum Model," J. Mech. Phys. Solids, 146, p. 104212.
[27] Treloar, L. R. G., 1943, "The Elasticity of a Network of Long-Chain Molecules—II," Trans. Faraday Soc., 39, pp. 241–246.
[28] Arruda, E. M., and Boyce, M. C., 1993, "A Three-Dimensional Constitutive Model for the Large Stretch Behavior of Rubber Elastic Materials," J. Mech. Phys. Solids, 41(2), pp. 389–412.
[29] Wu, P. D., and van der Giessen, E., 1992, "On Improved 3-D Non-Gaussian Network Models for Rubber Elasticity," Mech. Res. Commun., 19(5), pp. 427–433.
[30] Miehe, C., Göktepe, S., and Lulei, F., 2004, "A Micro-Macro Approach to Rubber-Like Materials—Part I: the Non-Affine Micro-Sphere Model of Rubber Elasticity," J. Mech. Phys. Solids, 52(11), pp. 2617–2660.
[31] Diani, J., Brieu, M., and Vacherand, J. M., 2006, "A Damage Directional Constitutive Model for Mullins Effect With Permanent Set and Induced Anisotropy," Eur. J. Mech. - A/Solids, 25(3), pp. 483–496.
[32] Diani, J., and Le Tallec, P., 2019, "A Fully Equilibrated Microsphere Model With Damage for Rubberlike Materials," J. Mech. Phys. Solids, 124(March), pp. 702–713.
[33] Göktepe, S., and Miehe, C., 2005, "A Micro–Macro Approach to Rubber-Like Materials. Part III: The Micro-Sphere Model of Anisotropic Mullins-Type Damage," J. Mech. Phys. Solids, 53(10), pp. 2259–2283.
[34] Miehe, C., and Göktepe, S., 2005, "A Micro–Macro Approach to Rubber-Like Materials. Part II: The Micro-Sphere Model of Finite Rubber Viscoelasticity," J. Mech. Phys. Solids, 53(10), pp. 2231–2258.
[35] Govindjee, S., Zoller, M. J., and Hackl, K., 2019, "A Fully-Relaxed Variationally-Consistent Framework for Inelastic Micro-Sphere Models: Finite Viscoelasticity," J. Mech. Phys. Solids, 127, pp. 1–19.
[36] Skrzeszewska, P. J., Sprakel, J., de Wolf, F. A., Fokkink, R., Cohen Stuart, M. A., and van der Gucht, J., 2010, "Fracture and Self-Healing in a Well-Defined Self-Assembled Polymer Network," Macromolecules, 43(7), pp. 3542–3548.
[37] Vernerey, F. J., 2018, "Transient Response of Nonlinear Polymer Networks: A Kinetic Theory," J. Mech. Phys. Solids, 115, pp. 230–247.
[38] Kuhn, W., and Grün, F., 1942, "Beziehungen Zwischen Elastischen Konstanten Und Dehnungsdoppelbrechung Hochelastischer Stoffe," Kolloid-Zeitschrift, 101(3), pp. 248–271.
[39] James, H. M., and Guth, E., 1943, "Theory of the Elastic Properties of Rubber," J. Chem. Phys., 11(10), pp. 455–481.
[40] Cohen, A., 1991, "A Padé Approximant to the Inverse Langevin Function," Rheol. Acta, 30(3), pp. 270–273.
[41] Bell, G. I., 1978, "Models for the Specific Adhesion of Cells to Cells," Science, 200(4342), pp. 618–627.
[42] Shen, T., Long, R., and Vernerey, F., 2019, "Computational Modeling of the Large Deformation and Flow of Viscoelastic Polymers," Comput. Mech., 63(4), pp. 725–745.
[43] Treloar, L. R. G., 1954, "The Photoelastic Properties of Short-Chain Molecular Networks," Trans. Faraday Soc., 50(0), pp. 881–896.
[44] Wu, P. D., and Van Der Giessen, E., 1993, "On Improved Network Models for Rubber Elasticity and Their Applications to Orientation Hardening in Glassy Polymers," J. Mech. Phys. Solids, 41(3), pp. 427–456.
[45] Holzapfel, G. A., 2000, Nonlinear Solid Mechanics: A Continuum Approach for Engineering Science, Wiley, Chichester.
[46] Treloar, L. R. G., 1975, The Physics of Rubber Elasticity, Oxford University Press, USA, Dec. Google-Books-ID: EfCZXXKQ50wC.
[47] Mao, Y., Talamini, B., and Anand, L., 2017, "Rupture of Polymers by Chain Scission," Extreme Mech. Lett., 13, pp. 17–24.
[48] Vernerey, F., Liu, W. K., and Moran, B., 2007, "Multi-Scale Micromorphic Theory for Hierarchical Materials," J. Mech. Phys. Solids, 55(12), pp. 2603–2651.
[49] Henderson, K. J., Zhou, T. C., Otim, K. J., and Shull, K. R., 2010, "Ionically Cross-Linked Triblock Copolymer Hydrogels With High Strength," Macromolecules, 43(14), pp. 6193–6201.
[50] Boyce, M. C., and Arruda, E. M., 2000, "Constitutive Models of Rubber Elasticity: A Review," Rubber Chem. Technol., 73(3), pp. 504–523.
[51] Bazant, P., and Oh, B. H., 1986, "Efficient Numerical Integration on the Surface of a Sphere," ZAMM – Journal of Applied Mathematics and Mechanics/ Zeitschrift für Angewandte Mathematik und Mechanik, 66(1), pp. 37–49. _eprint: https://onlinelibrary.wiley.com/doi/pdf/10.1002/zamm.19860660108.
[52] Anderson, A. J., Culver, H. R., Bryant, S. J., and Bowman, C. N., 2020, "Viscoelastic and Thermoreversible Networks Crosslinked by Non-Covalent Interactions Between "Clickable" Nucleic Acid Oligomers and DNA," Polym. Chem., 11(17), pp. 2959–2968.